Laboratory versus intrinsic description of nonaxial nuclei above doubly magic ^{78}Ni

K. Sieja,[1] T. R. Rodríguez,[2] K. Kolos,[3,4] and D. Verney[3]
[1]*Université de Strasbourg, IPHC, CNRS, UMR7178, 67037 Strasbourg, France*
[2]*Institut für Kernphysik, Technische Universität Darmstadt, Schlossgartenstr. 2, D-64289 Darmstadt, Germany*
[3]*Institut de Physique Nucléaire, CNRS/IN2P3 and Université Paris Sud, Orsay, France*
[4]*University of Tennessee, Knoxville, Tennessee 37996, USA*
(Received 2 August 2013; revised manuscript received 28 August 2013; published 30 September 2013)

We study the development of collectivity in neutron rich nuclei in the close vicinity of ^{78}Ni. We report on the large scale shell model calculations in the $N = 52$–54 even-even nuclei with $Z = 30$–36. We predict maximum of triaxiality in ^{86}Ge and explain this phenomenon on the basis of a pseudo-SU(3) symmetry interpretation. For the cases where signs for nonaxial shapes appear, we perform the triaxial Gogny calculations with particle number and angular momentum projections. The comparison of results obtained in the laboratory and intrinsic frames provides a comprehensive and complete picture of nuclear deformation in this region.

DOI: 10.1103/PhysRevC.88.034327 PACS number(s): 21.60.Cs, 21.60.Jz, 23.20.Lv, 21.10.−k

I. INTRODUCTION

The study of collective behavior of deformed nuclei is a classical problem in nuclear physics. Mean-field descriptions in the intrinsic frame are perfectly suited for such studies, as they take advantage of the spontaneous breaking of rotational symmetry. The price to pay for the gain in the physical insight is the loss of angular momentum as a good quantum number. On the contrary, in the nuclear shell model defined in the laboratory frame, angular momentum is conserved but the physical insight associated with the existence of the intrinsic state is lost. However, in the cases of well-deformed nuclei, such as ^{24}Mg or ^{48}Cr, the collective properties in shell model can be traced back to the validity of the Eliott's SU(3) symmetry, for which the relationship between the intrinsic and laboratory frame descriptions is well understood.

The region of neutron-rich nuclei above the $N = 50$ shell closure appears particularly interesting for the study of the quadrupole properties. From the shell model point of view, the nuclei above ^{78}Ni can be described in a model space comprising neutron ($2d_{5/2}$, $3s_{1/2}$, $2d_{3/2}$, $1g_{7/2}$, $1h_{11/2}$) and proton ($1f_{5/2}$, $2p_{3/2}$, $2p_{1/2}$, $1g_{9/2}$) orbitals. These two sets of orbits contain those connected by a strong quadrupole interaction and can form the pseudo-SU(3) blocks. Approaching the SU(3) limit would require a degeneracy or a close proximity of the orbitals of interest. From the shell model extrapolations it appears that at least the $2d_{5/2}$ and $3s_{1/2}$ are degenerate in ^{78}Ni [1] and that proton $1f_{5/2}$ and $2p_{3/2}$ orbits cross around $Z = 28$ with the filling of the $g_{9/2}$ neutron orbital [2]. Thus, while ^{78}Ni itself is predicted to be closed shell nucleus in the shell model picture [3], as soon as few protons and neutrons are added the deformation can set up quickly. Mean-field, Hartree-Fock-Bogoliubov (HFB) calculations with Gogny forces [4], revealed a possibility of shape mixing in this region and indicate a non-negligible role of the nonaxial degrees of freedom in ground states of these nuclei. Nevertheless, beyond-mean field calculations are needed to provide spectroscopic information to be compared with the experimental data and with other theoretical approaches. In particular, the recently developed full triaxial angular momentum restoration and shape mixing with Skyrme [5], relativistic mean-field [6], and Gogny [7] energy density functionals are the perfect tools to study these collective phenomena all over the nuclear chart.

The experimental studies in the region around ^{78}Ni has been also intense in the recent years. While it is still difficult to study the structure of ^{78}Ni itself at currently existing facilities, the knowledge of the light $N = 50$–54 even-even isotones has been extended down to $Z = 30$ for $N = 50$ [8], $Z = 32$ for $N = 52$ [9,10], and $Z = 34$ for $N = 54$ [11]. In particular, the first possible signs of deformation at $N = 52$ have been reported in Ref. [9], where the excited levels of ^{84}Ge have been observed. The comparison with five-dimensional collective Hamiltonian (5DCH) calculations [12] pointed to a certain softness of this nucleus. The detailed spectroscopy of ^{80}Ge clearly reveals the existence of γ-soft collective structures at $N = 48$ [13]. The question that arises now is to understand wether this behavior is maintained after the $N = 50$ shell closure, in the natural valence space above the ^{78}Ni core, and why. Recently, the first observation of excited levels of ^{87}Se ($N = 53$) has been achieved [14]. The adjacent shell model interpretation in such a valence space has suggested the increased collectivity of this nucleus to be responsible for the observed level ordering.

In this work we perform a shell model study of even-even $N = 52$–54 isotopes with $Z = 30$–36 and we focus on the quadrupole properties of these nuclei as seen in the laboratory system. We interpret our results using the limits of the Eliott's SU(3) symmetry in its pseudo-SU(3) variant. In the selected cases, where signs of deformation and triaxiality are present in the shell model framework, we also perform symmetry conserved configuration mixing (SCCM)-Gogny calculations. Our work is organized as follows. First we discuss details of the shell model calculations in Sec. II A and we analyze the limits of the quadrupole deformation of considered systems in a pseudo-SU(3) symmetry model in Sec. II B. We outline the SCCM-Gogny approach with particle number and angular momentum projections in Sec. II C. In Sec. III we gather the quadrupole properties obtained in microscopic shell model

calculations for the ensemble of considered nuclei and then we discuss in more detail selected cases, in comparison with the results of the SCCM-Gogny approach. Finally, we collect our main conclusions in Sec. IV.

II. THEORETICAL FRAMEWORK

A. Shell model: Valence space and interaction

The shell model calculations presented in this work has been achieved in a model space $\pi(1f_{5/2}, 2p_{3/2}, 2p_{1/2}, 1g_{9/2})$ and $\nu(2d_{5/2}, 3s_{1/2}, 2d_{3/2}, 1g_{7/2}, 1h_{11/2})$ outside the ^{78}Ni core, which we name $\pi r3g - \nu r4h$ (following notation of Ref. [15]). The effective interaction used in this model space has been established and described in Ref. [1]. It contains a fit from Ref. [16] in its proton-proton part, the neutron-neutron interaction called GCN5082 [17–19] and the proton-neutron realistic G-matrix constrained in its monopole part to reproduce the shell evolution between ^{91}Zr and ^{101}Sn. It has been originally conceived to study the zirconium isotopes but it appeared also quite successful for the description of low lying and isomeric states in lighter Z nuclei [20–23]. Recently it has been applied to the study of the yrast excitations in $N = 52$ nuclei from $Z = 30$ to $Z = 44$ and in particular, to the evolution of the $4^+ - 6^+$ splitting in these systems. The latter appeared to be reproduced in a great detail in the present shell model approach, confirming its validity also in the closer vicinity of ^{78}Ni [24]. Also a study of $N = 53$ isotones has been achieved within the same framework [14], where shell model has been successful in interpreting the low energy levels systematics and in particular, the descending trend of the $3/2^+$ state between ^{93}Zr and ^{87}Se. A development of deformation in the proton midshell has been suggested to cause the observed ordering of levels in ^{87}Se.

In this work we consider even-even systems having two to six protons and two to four neutrons in the valence space, i.e., the $N = 52, 54$ isotones with $Z = 30$–36. The m-scheme dimensions for these nuclei do not exceed 2×10^8. Full space diagonalizations of such systems using the m-scheme shell model code ANTOINE [25] are not computationally intense at all and can be performed on a laptop.

In the calculations of quadrupole moments and transition rates, we have used an enhanced polarization charge of $0.7e$, as suggested previously in Ref. [1] for this model space. This allows us, in particular, to account for the missing proton excitations from the $f_{7/2}$ orbital to the rest of the shell, crucial in nuclei around $Z = 28$, $N = 50$ [2], and thus to match better the measured $B(E2; 2^+ \to 0^+)$ values of $N = 50$ nuclei: ^{80}Zn and ^{86}Kr. The enhanced neutron polarization charge can account for the missing excitations from the $g_{9/2}$ orbital.

To provide some more insight on the intrinsic shape associated to the calculated shell model states, the $E2$ matrix elements were analyzed following the same method which is applied in multiple Coulomb excitation formalism. For this purpose we use the model independent n-body quadrupole moments introduced in Ref. [26] in a similar way as was already done in Ref. [13]. For the sake of clarity we shall remind here the expressions for the two-body and three-body quadrupole moments of a given state $s \equiv (s, I_s, \Pi_s)$ (as calculated here from shell model results):

$$p_s^{(2)} = (2I_s + 1)^{-1} \sum_r M_{sr}^2 = \frac{5(I_s + 1)(2I_s + 3)}{16\pi I_s(2I_s - 1)} Q_{\rm spec}^2(s) + \sum_{r \neq s} B(E2; s \to r), \quad (1)$$

where M_{sr} are the reduced $E2$ matrix elements,

$$p_s^{(3)} = -\sqrt{5}(2I_s + 1)^{-1}(-1)^{2I_s} \times \sum_{rt} \begin{Bmatrix} 2 & 2 & 2 \\ I_s & I_r & I_t \end{Bmatrix} M_{sr} M_{rt} M_{ts}, \quad (2)$$

where r and t are the intermediate (shell model here) states connected by $E2$ transitions to the state s considered and M_{ij} are the $E2$ reduced matrix elements between states s, r, and t. These are completely general and model independent measures of the the intrinsic axial deformation and asymmetry, being related to parameters of an equivalent ellipsoid having the same $p_s^{(2)}$ and $p_s^{(3)}$ moments by:

(i) for the intrinsic quadrupole moment $Q_{\rm int}(s)$ (from which the axial deformation parameter $\beta(s)$ is extracted):

$$Q_{\rm int}(s) = \sqrt{\frac{16\pi}{5} p_s^{(2)}}, \quad (3)$$

(ii) for the asymmetry angle $\gamma(s)$:

$$\cos 3\gamma(s) = -\sqrt{7/2}\, p_s^{(3)} \left(p_s^{(2)}\right)^{-3/2}. \quad (4)$$

B. Pseudo SU(3) model analysis of quadrupole moments

The quadrupole properties of nuclei contained in the valence space $\pi r3g$-$\nu r4h$ can be anticipated by looking into the limits of the pure pseudo-SU(3) symmetry first proposed by Arima [27] and applied, e.g., in Refs. [1,15,18]. In this work we investigate the nuclei for which the essential features should be described within the $pf_{5/2}$ orbits on the proton side and $dg_{7/2}s_{1/2}$ on the neutron side, thus we can consider having pseudo-SU(3) blocks for protons (pseudo-sd) and for neutrons (pseudo-pf). The quadrupole properties of the Nilsson-like orbitals of a pseudo-SU(3) in a shell with principal quantum number $n + 1$ are the same as those of the SU(3) orbits with principal quantum number n, for which the intrinsic quadrupole moment is given by [15]:

$$q_0(n, \chi, k) = -(2n - 3\chi)b^2, \quad (5)$$

where χ can take integer values between 0 and n, $k = \pm(\frac{1}{2}, \ldots, \frac{1}{2} + \chi)$, and b is the harmonic oscillator length parameter. The total intrinsic quadrupole moment Q_0 is obtained as a sum of all the contributions from the valence particles with corresponding effective charges. In this scheme the energy is proportional to Q_0^2 thus the orbits are filled starting from $\chi = 0$ or $\chi = n$ in a way which maximizes the absolute value of the intrinsic quadrupole moment.

Let us start with two or four neutrons occupying the pseudo-pf orbits. Two neutrons maximize the quadrupole deformation when they occupy the lowest $\chi = 0$ orbital with $k = 1/2$ and

$k = -1/2$, leading to the total $K = \sum k = 0$. Four neutrons can be distributed in several degenerate configurations:

$$(\chi = 0, k = \pm 1/2)^2 (\chi = 1, k = \pm 1/2)^2,$$
$$(\chi = 0, k = \pm 1/2)^2 (\chi = 1, k = \pm 3/2)^2,$$
$$(\chi = 0, k = \pm 1/2)^2 (\chi = 1, k = \pm 1/2)^1 (\chi = 1, k = \pm 3/2)^1,$$

which means a possibility of $K = 0$ and $K = 2$. Even a small mixing of $K = 0$ and $K = 2$ would lead to triaxiality: such a mixing is impossible in a pure pseudo-SU(3) limit but may appear in realistic shell model calculations.

Moving to the proton side, we need to consider two, four, six, or eight valence protons in the pseudo-sd block, which will correspond to Zn, Ge, Se, and Kr nuclei in our model space. The two valence protons of Zn maximize the quadrupole moment when they occupy both the lowest $\chi = 0$ orbital (total $K = 0$). The situation of Ge becomes more complex as the four valence protons can adopt several degenerate configurations:

$$(\chi = 0, k = \pm 1/2)^2 (\chi = 1, k = \pm 1/2)^2,$$
$$(\chi = 0, k = \pm 1/2)^2 (\chi = 1, k = \pm 3/2)^2,$$
$$(\chi = 0, k = \pm 1/2)^2 (\chi = 1, k = \pm 1/2)^1 (\chi = 1, k = \pm 3/2)^1,$$

leading to possible $K = 0$ and $K = 2$. The same analysis in Se (six particles) gives a possibility of two degenerate cases with $K = 0$ having the same Q_0 values, but with opposite signs:

$$(\chi = 0, k = \pm 1/2)^2 (\chi = 1, k = \pm 1/2)^2 (\chi = 1, k = \pm 3/2)^2,$$
$$(\chi = 2, k = \pm 1/2)^2 (\chi = 2, k = \pm 3/2)^2 (\chi = 2, k = \pm 5/2)^2.$$

Similarly, eight particles (Kr) can be redistributed in several degenerate configurations, again with $K = 0, 2$.

The values of total intrinsic quadrupole moments and corresponding $B(E2)$ values obtained in the pseudo-SU(3) limit [using Eq. (10)] are summarized in Table I. The polarization charge of $0.7e$ is used in the pseudo-SU(3) model to make comparisons with SM calculations straightforward.

The major conclusions from the pseudo-SU(3) model analysis are the following: The degenerate configurations with $K = 0$ and $K = 2$ can be obtained for four and eight protons and for four neutrons in the valence space. Thus one may expect some triaxiality in realistic calculations and in experiment, reaching its maximum in ^{86}Ge. The largest axial deformation is predicted for six protons and four neutrons in the valence space (^{88}Se).

TABLE I. Predictions of the pseudo-SU(3) symmetry limit for the values of intrinsic quadrupole moments (in $e$fm^2) and $B(E2; 2^+ \to 0^+)$ transition values (in e^2fm^4) in the studied nuclei.

Nucleus	Q_0	$B(E2; 2^+ \to 0^+)$	Nucleus	Q_0	$B(E2; 2^+ \to 0^+)$
^{82}Zn	114	258	^{84}Zn	135	362
^{84}Ge	131	342	^{86}Ge	151	454
^{86}Se	148	436	^{88}Se	168	561
^{88}Kr	117	272	^{90}Kr	137	373

TABLE II. Properties of the yrast band of $N = 52$ isotones [energies in MeV, quadrupole moments in $e$fm^2, $B(E2)$ in e^2fm^4]. The calculations are done in the $\pi r3g$-$\nu r4h$ model space with $1.7e$ and $0.7e$ effective charges for protons and neutrons, respectively.

Z	J	E^*	$B(E2; J \to J-2)$	$Q_{\rm spec}$	Q_0 from $B(E2)$	Q_0 from $Q_{\rm spec}$	β
30	2^+	0.88	169	− 14	92	48	
	4^+	1.50	127	− 24	67	66	
	6^+	3.17	182	− 40	77	100	
32	2^+	0.75	371	− 27	136	93	
	4^+	1.56	364	− 37	113	101	
	6^+	3.03	455	− 27	120	67	
34	2^+	0.70	436	− 37	148	129	0.19
	4^+	1.41	439	− 46.5	124	128	0.17
	6^+	2.76	607	− 55	139	136	0.19
36	2^+	0.88	329	6.5	129	23	
	4^+	1.66	207	− 31	85	86	
	6^+	3.24	95	14	55	35	

C. Details of symmetry conserving configuration mixing–Gogny calculations

In this section we describe briefly the beyond mean-field method used in this work. In this approach, we use the generator coordinate method (GCM) to define the many-body wave functions [28]. Hence, we consider linear combinations of states with different intrinsic quadrupole deformations, axial and triaxial [5,7]:

$$|JM; NZ; \sigma\rangle = \sum_{\beta,\gamma,K} f^{J;NZ;\sigma}_{\beta,\gamma,K} |JMK; NZ; \beta\gamma\rangle, \qquad (6)$$

where N, Z, J, M, K are the number of neutrons and protons, the total angular momentum and the angular momentum component on the z axes of the laboratory and fixed frames, respectively. The quadrupole deformation is parametrized by the (β, γ) coordinates and the states $|JMK; NZ; \beta\gamma\rangle$ are found by performing particle number and angular momentum

TABLE III. Properties of the yrast band of $N = 54$ isotones [energies in MeV, quadrupole moments in $e$fm^2, $B(E2)$ in e^2fm^4].

Z	J	E^*	$B(E2; J \to J-2)$	$Q_{\rm spec}$	Q_0 from $B(E2)$	Q_0 from $Q_{\rm spec}$	β
30	2^+	0.80	193	− 26	98	91	
	4^+	1.50	93	3.5	57	10	
	6^+	2.83	139	− 52	67	131	
32	2^+	0.65	465	− 40	153	140	0.21
	4^+	1.75	628	− 40	149	110	0.19
	6^+	3.26	659	− 33	145	82	0.17
34	2^+	0.67	568	− 48	169	168	0.23
	4^+	1.94	714	− 54	158	148	0.21
	6^+	3.58	466	− 55	122	137	0.18
36	2^+	0.80	386	− 24	139	84	
	4^+	1.75	201	20	84	55	
	6^+	3.15	447	48	119	121	

TABLE IV. Excited bands of selected $N = 52$ isotones [energies in MeV, quadrupole moments in $e$fm^2, $B(E2)$ in e^2fm^4].

Z	J	E^*	$B(E2; J \to J-1)$	$Q_{\rm spec}$
30	2_2^+	1.86		0.7
	3^+	2.46	23	− 20
	4_2^+	2.43	10	− 32
	5^+	3.11	40	− 19
32	2_2^+	1.54		26
	3^+	2.12	639	− 4
	4_2^+	2.31	366	− 22
	5^+	2.96	200	− 28
34	2_2^+	1.64		5
	3^+	2.25	523	− 10
	4_2^+	2.71	27	− 38
	5^+	3.50	118	− 30
36	2_2^+	1.72		− 5
	3^+	2.52	214	− 10
	4_2^+	2.28	11	55
	5^+	3.17	108	− 9

projection of HFB wave functions $|\Phi(\beta, \gamma)\rangle$:

$$|JMK; NZ; \beta\gamma\rangle = P^J_{MK} P^N P^Z |\Phi(\beta, \gamma)\rangle. \quad (7)$$

Here, P^J_{MK}, P^N, and P^Z are the operators that project onto good angular momentum and number of particles, respectively [28]. The HFB wave functions are found by minimizing the particle number projected HFB energy (PN-VAP method [29]) using constraints on the quadrupole degrees of freedom to produce a set of states with the desired deformation. In this work we use for each nucleus a mesh of 72 states with deformations ranges as follows: ($\beta \in [0.0, 0.8]$, $\gamma \in [0^\circ, 60^\circ]$). In addition, the HFB wave functions preserve time-reversal and spatial parity symmetries (only positive parity states can be described) and are expanded in a spherical harmonic oscillator basis including nine major oscillator shells. Finally, the minimization of the energy computed with the GCM states given in Eq. (6) is equivalent to solving the Hill-Wheeler-Griffin (HWG) equations:

$$\sum_{\beta_2', \gamma', K'} \left(\mathcal{H}^{J;NZ}_{\beta,\gamma,K;\beta_2',\gamma',K'} - E^{J;NZ;\sigma} \mathcal{N}^{J;NZ}_{\beta,\gamma,K;\beta_2',\gamma',K'} \right) f^{J;NZ;\sigma}_{\beta_2',\gamma',K'} = 0, \quad (8)$$

where $\mathcal{H}^{J;NZ}_{\beta,\gamma,K;\beta_2',\gamma',K'}$ and $\mathcal{N}^{J;NZ}_{\beta,\gamma,K;\beta_2',\gamma',K'}$ are the energy and norm overlap kernels, respectively. From the solution of the HWG equations we obtain directly the energy spectrum $E^{J;NZ;\sigma}$ ($\sigma = 1, 2, 3, \ldots$) and the coefficients needed to compute expectation values and electromagnetic transitions among the different states. The number of integration points both in gauge and Euler angles for particle number and angular momentum projection, the size of the harmonic oscillator basis, as well as the number of mesh points in the triaxial plane are chosen to ensure the convergence in the expectation values, transition rates and collective wave functions computed in this work. Further details about the performance of the method can be found in Ref. [7]. The main differences with the 5DCH method [12] are: i) exact GCM calculations without gaussian overlap approximation (GOA) are performed, ii) exact symmetry restoration (particle number and angular momentum) is accomplished, iii) the set of intrinsic HFB wave functions is found in the PN-VAP method instead of using a plain HFB. The computations within SCCM approach are time consuming and take approximately twenty days for each nucleus on a cluster with 150 CPUs. Therefore, this method has been used only in the analysis of ^{86}Ge and ^{88}Se, where the role played by the triaxial degree of freedom is expected to be most relevant.

TABLE V. Excited bands of selected $N = 54$ isotones [energies in MeV, quadrupole moments in $e$fm^2, $B(E2)$ in e^2fm^4].

Z	J	E^*	$B(E2; J \to J-1)$	$Q_{\rm spec}$
30	2_2^+	1.43		21
	3^+	1.94	132	− 1
	4_2^+	1.93	0.5	− 20
	5^+	2.81	1.4	− 8
32	2_2^+	1.39		39
	3^+	1.79	747	− 0.7
	4_2^+	2.34	214	3.5
	5^+	2.91	77	− 28
34	2_2^+	2.03		39
	3^+	2.41	583	− 6
	4_2^+	2.53	26	39
	5^+	3.31	234	− 25
36	2_2^+	1.35		27
	3^+	1.87	540	1.0
	4_2^+	2.25	44	14
	5^+	3.0	5	11

III. RESULTS

A. Deformation properties of $N = 52$–54 isotones in the laboratory picture

We start the discussion with the results obtained in the shell model framework. In Tables II and III we collect the properties of the investigated systems which characterize quadrupole properties of the yrast bands: energies, $B(E2)$ values, and spectroscopic quadrupole moments $Q_{\rm spec}$. We derive the intrinsic quadrupole moments Q_0 from the spectroscopic ones using the well known relations:

$$Q_0 = \frac{(J+1)(2J+3)}{3K^2 - J(J+1)} Q_{\rm spec}(J), \quad K \neq 1 \quad (9)$$

and

$$B(E2; J \to J-2) = \frac{5}{16\pi} e^2 \frac{(J+1)(J+2)}{(2J+3)(2J+5)} Q_0^2, \quad (10)$$

for $K \neq 1/2, 1$.

Let us also remind, that a γ band ($K = 2$), apart of a characteristic level sequence, has $Q(2_\gamma^+) = -Q(2_\gamma^+)$ and $Q(3^+) \sim 0$. In the Davidov-Filipov model [30] the amount of the triaxiality is derived from the ratio:

$$\frac{B(E2; 2_\gamma^+ \to 2_y^+)}{B(E2; 2_\gamma^+ \to 0_y^+)}, \quad (11)$$

TABLE VI. Intrinsic shape parameters of the shell model states.

(Yrast)	State	Q_0	β	γ (deg.)	Q_0(SU3)	$Q_0^{\rm rot}$	$\beta^{\rm rot}$
^{86}Ge	$0^+_{\rm g.s.}$	165	0.238	12	151	–	–
	2^+_1	161	0.232	8		153/140	0.21
	4^+_1	152	0.218	12		149/110	0.19
	6^+_1	118	0.172	10		145/82	0.17
^{88}Se	$0^+_{\rm g.s.}$	174	0.250	9	168	–	–
	2^+_1	169	0.243	12		169/168	0.23
	4^+_1	159	0.229	15		158/148	021
	6^+_1	118	0.173	14		122/137	0.18
(Excited)	State	Q_0	β	γ (deg.)			
^{86}Ge	2^+_2	152	0.219	28			
	3^+_1	148	0.213	32			
	4^+_2	116	0.169	41			
	5^+_1	105	0.154	33			
^{88}Se	2^+_2	152	0.219	35			
	3^+_1	143	0.207	36			
	4^+_2	114	0.166	40			
	5^+_1	100	0.146	36			

where y subscript denotes the yrast states. In Tables IV and V we collect the quantities characterizing the excited bands in several nuclei.

As can be seen, the yrast bands of $N = 52$ zinc, germanium and krypton miss the characteristic features of deformed bands: The inequality of quadrupole moments derived from spectroscopic moments and from transition values assuming $K = 0$, as well as the visible variation of the derived quantities with spin, do not allow us to associate the intrinsic deformation parameter to this band. This situation gets different in selenium, where the features of ground state deformation are present. The results are compatible with a deformed intrinsic state with nearly constant quadrupole moment $Q_0 \sim 130\, e\text{fm}^2$, corresponding to $\beta \sim 0.19$ for ^{86}Se. The SM results confirm the analytic pseudo-SU(3) model predictions that the maximum of deformation is obtained with six protons in the model space, thus in ^{86}Se for $N = 52$. Also qualitative agreement between the pseudo-SU(3) and realistic SM quadrupole moments is reasonable.

From Table III one has clear evidence for sizable deformation of Ge and Se at $N = 54$. The full calculation of the intrinsic shape parameters using the n-body quadrupole operators was done for the yrast $0^+_{\rm g.s.}, 2^+_1, 4^+_1, 6^+_1$ sequence and for the excited band $2^+_2, 3^+_1, 4^+_2, 5^+_1$. The results are summarized in Table VI and compared to the pseudo-SU(3) predictions and results from the simpler axial rotor analysis of Table III. These two bands, with their main $E2$ connections, are also displayed in Fig. 1(a) and 1(b).

Concerning the yrast sequence, a very nice agreement is found for the results obtained with the three different methods. This means that the collectivity originates mainly from the global rotation of the shape, with the triaxial degree of freedom playing only a marginal role. But this collective axial feature stops already at 6^+ both in ^{86}Ge and ^{88}Se, showing that the axial collectivity is not yet fully established and that those nuclei mark the beginning of full shell collectivity or the end of a transitional region. All three methods consistently depict ^{88}Se as more collective than ^{86}Ge which is expected, as ^{88}Se is closer to the proton mid shell. The ground state axial deformation parameter β in particular is stronger in ^{88}Se than in ^{86}Ge. The second part of Table VI contains the results for the nonyrast sequence built on top of the 2^+_2 state. The asymmetry angles of all states considered are close to 30°, this band is clearly characteristic of a triaxial structure and the comparison with the SU(3) or axial rotor limit cannot help. Nor can the comparison with the Davidov and Filipov model as the calculation of the higher order n-body quadrupole moments rather reveals γ instability than

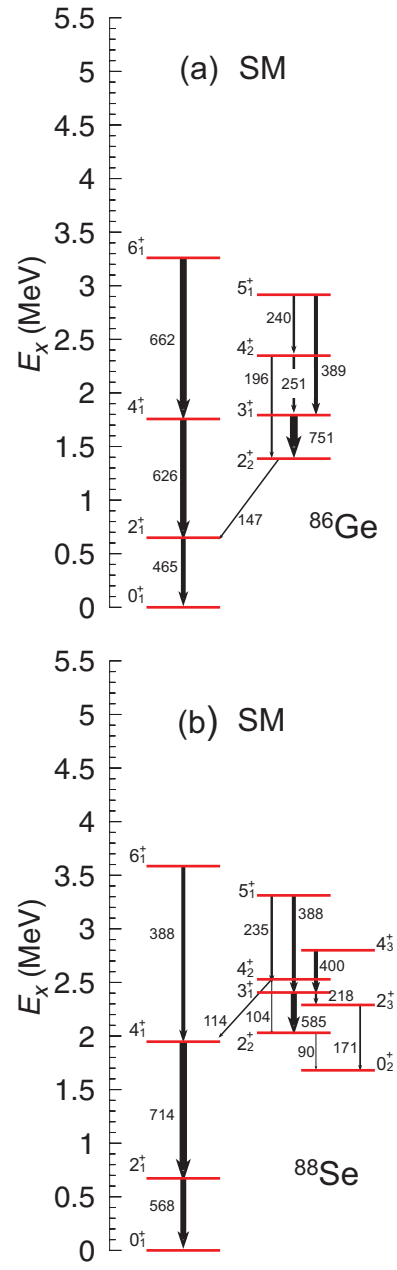

FIG. 1. (Color online) Excitation energies (in keV) and highest reduced transition rates $B(E2)$ (in $e^2\text{fm}^4$) for (a) ^{86}Ge and (b) ^{88}Se, calculated in the shell model framework.

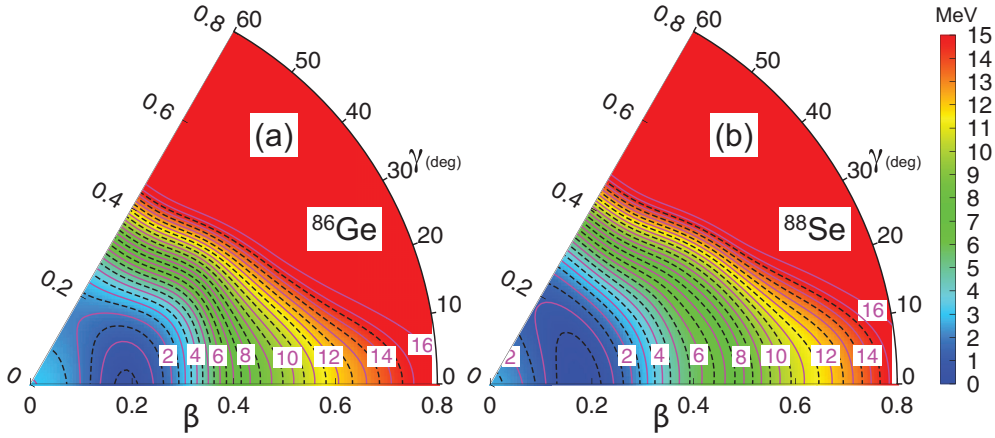

FIG. 2. (Color online) Potential energy surfaces in the particle number variation after projection (PN-VAP) approach along the (β, γ) plane for (a) ^{86}Ge and (b) ^{88}Se nuclei calculated with the Gogny D1S interaction.

permanently triaxially deformed, rotating shape. The axial parameters of the states forming this sequence are practically the same between the two nuclei, the difference comes from the asymmetry angle, higher in the case of ^{88}Se than in ^{86}Ge. One can consider that the triaxiality revealed by this band is maximum in ^{86}Ge while ^{88}Se is already leaning towards oblateness. A fact which, rather unexpectedly, is consistent with the SCCM results as will be shown in the following paragraph.

B. Intrinsic description of triaxial deformation

We now analyze the results obtained with the SCCM method described in Sec. II C for ^{86}Ge and ^{88}Se ($N = 54$) nuclei. To have an insight into the role of the intrinsic deformation in these isotopes we represent in Fig. 2 the potential energy surfaces (PES) along the triaxial (β, γ) plane in the PN-VAP approach. Here we observe that both nuclei have rather similar PES, with absolute minima at axial prolate deformations $\beta \sim 0.15$–0.20 and a quite flat region between $\beta \in [0.0, 0.3]$, $\gamma \in [0^\circ, 60^\circ]$. In addition, ^{88}Se shows a slightly more pronounced γ softness than ^{86}Ge, where the prolate minimum is better defined. This kind of soft potentials suggests that configuration mixing effects can play a key role in understanding the spectra for these nuclei. Hence, we now describe the results obtained by performing shape mixing calculations with particle number and angular momentum restored states. In Fig. 3 we represent the excitation energies and reduced transition probabilities $B(E2)$ for ^{86}Ge [Fig. 3(a)] and ^{88}Se [Fig. 3(b)]. The states are sorted by connecting the different levels with the ones with the larger values of the $B(E2)$. On the one hand, we obtain for both nuclei ground state (g.s.) bands with the sequence of angular momentum $0_1^+, 2_1^+, 4_1^+, 6_1^+$, which in principle indicates the presence of rotational bands. The mean value of the intrinsic third component of the angular momentum is mainly $K = 0$ for all the states belonging to these bands as we show in Table VII and VIII. The $r_{42} = E(4_1^+)/E(2_1^+)$ ratios ($r_{42} = 2.7$ and 2.6 for ^{86}Ge and ^{88}Se, respectively) for these states do not support the existence of

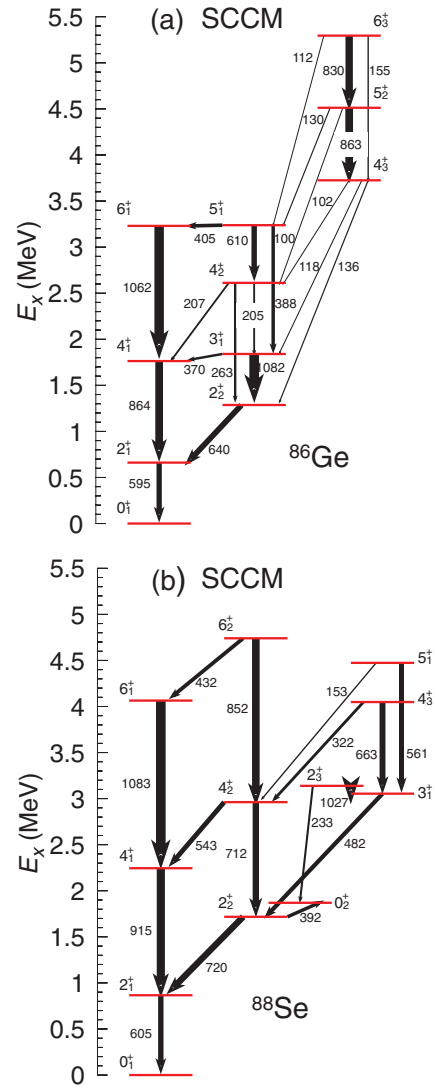

FIG. 3. (Color online) Excitation energies (in MeV) and highest reduced transition probabilities $B(E2)$ (in e^2fm^4) for (a) ^{86}Ge and (b) ^{88}Se calculated with the Gogny D1S interaction.

TABLE VII. Excitation energies (in MeV), spectroscopic quadrupole moments (in $e\text{fm}^2$) and distribution of the intrinsic quantum number K of the states for g.s., first, and second excited bands in ^{86}Ge.

	0_1^+	2_1^+	4_1^+	6_1^+	2_2^+	3_1^+	4_2^+	4_3^+	5_2^+
$E(J_\sigma^+)$	0.000	0.661	1.763	3.230	1.286	1.840	2.612	3.725	4.512
$Q_{\text{spec}}(J_\sigma^+)$	0.000	− 26.691	− 19.165	− 17.057	27.182	0.000	− 57.542	77.500	30.497
$K = 0$	1.000	0.858	0.695	0.561	0.222	0.000	0.261	0.166	0.000
$\|K\| = 2$	0.000	0.142	0.289	0.401	0.778	1.000	0.563	0.149	0.189
$\|K\| = 4$	0.000	0.000	0.016	0.036	0.000	0.000	0.176	0.685	0.811

well-deformed axial rotational bands in these cases. However, the ratios of $4^+/2^+$ energies, strongly dependent on the pairing interaction in nuclei, are hardly indicative for the rotational structures in lighter, even well deformed nuclei. For example, the experimental $E(4^+)/E(2^+)$ value in ^{20}Ne is 2.6, in ^{24}Mg 3.01 and 2.47 in ^{48}Cr, which is also far from the rotational limit value of 3.3. In Fig. 5 we thus represent the ratio of the spectroscopic quadrupole moments $Q_{\text{spec}}(J)/Q_{2^+}$. The 2^+ states vary for each band, and for the ground state bands we see a distinctive deviation from the rotational limit. The main difference between the two isotones is however found in the first and second excited bands. For ^{86}Ge we obtain a $2_2^+, 3_1^+, 4_2^+, 5_1^+$ band (predominantly $K = 2$) strongly connected to the g.s. band and another one with the sequence $4_3^+, 5_2^+, 6_3^+$ (mostly $K = 4$) with smaller $B(E2)$ values both towards the g.s. and first excited bands. On the other hand, ^{88}Se presents a much more mixed band structure as we see in Fig. 3(b). In this case, we find the state 2_2^+ at a slightly lower excitation energy than the 0_2^+ and with a large $B(E2)$ between them. These two states together with $4_2^+, 6_2^+$ develop a $K = 0$ band strongly connected to the g.s. band. In addition, we have also a predominantly $K = 2$ band $(3_1^+, 2_3^+, 4_3^+, 5_1^+)$ with a small admixture of $K = 0$ components that is also connected to the first excited band.

To shed light on the shape structure of these states we represent in Fig. 4 the collective wave functions for the band-head states described above. The rest of the states belonging to the same band have a similar distribution. The maxima in the probabilities are found at $(\beta \sim 0.2, \gamma = 0°)$, $(\beta \sim 0.25, \gamma = 15°)$, and $(\beta \sim 0.25, \gamma = 18°)$ for ^{86}Ge and at $(\beta \sim 0.2, \gamma = 0°)$, $(\beta \sim 0.25, \gamma = 60°)$, and $(\beta \sim 0.2, \gamma = 28°)$ for ^{88}Se. We observe that in most of the states represented in Fig. 4 the probability is distributed in a range of deformations $(\beta \in [0.10, 0, 35], \gamma \in [0°, 60°])$ showing that the triaxial degree of freedom plays an important role, specially for the states in the first and second exited bands. Finally, we notice that the ground state of ^{88}Se is slightly more spherical than the g.s. of ^{86}Ge, consistently having a larger $E(2_1^+)$ (see Fig. 3).

C. Comparison of SM and SCCM calculations for ^{86}Ge and ^{88}Se

The comparison of calculated spectra and transition rates in shell model and beyond mean-field frameworks is done based on results shown in Figs. 1(a) and 3(a) for ^{86}Ge and Figs. 1(b) and 3(b) for ^{88}Se. The comparison of deformation properties in both models is shown in Fig. 5, where the ratios of spectroscopic moments are plotted and compared to those of the rotational limit.

For ^{86}Ge, an excellent agreement between the two models is found for predicted excitation energies. They agree in the two calculations within several keV for the yrast band and within 300 keV for the first excited band. Both models are as well consistent in their description of the relative magnitudes of the intraband transitions. However, shell model predicts two rather disconnected bands: the $B(E2)$ values between the first excited and the ground state band are severely quenched with respect to intraband transitions, except of the $2_2^+ \to 2_1^+$ one, which is the only plotted in the Fig. 1(a). In the SCCM calculations the out-band transitions are closer in magnitude to the intraband ones.

One should note that the absolute magnitude of transition rates is overall much stronger in the SCCM calculations than in the shell model. It appears that SCCM overshoots the transition rate in the neighboring $N = 50$ ^{86}Kr nucleus, where the experimental data is available: 336 $e^2\text{fm}^4$ is calculated against the experimental value of 244(20) $e^2\text{fm}^4$. Nonetheless, the trends of excitation energies and transition rates along the Kr chain in the known region are correctly reproduced in SCCM calculations. Shell model $B(E2)$ values for $N = 50$ are much closer to experimental ones: we obtain 121 $e^2\text{fm}^4$ for ^{80}Zn and 262 $e^2\text{fm}^4$ for ^{86}Kr, while the experimental values are 146(18) $e^2\text{fm}^4$ and 244(20) $e^2\text{fm}^4$, respectively. The good

TABLE VIII. Same as Table VII but in ^{88}Se.

	0_1^+	2_1^+	4_1^+	6_1^+	0_2^+	2_2^+	4_2^+	2_3^+	3_1^+
$E(J_\sigma^+)$	0.000	0.866	2.245	4.740	1.869	1.717	2.962	3.139	3.054
$Q_{\text{spec}}(J_\sigma^+)$	0.000	− 22.730	− 19.789	− 0.261	0.000	25.374	9.750	− 36.351	0.000
$K = 0$	1.000	0.941	0.888	0.771	1.000	0.728	0.853	0.393	0.000
$\|K\| = 2$	0.000	0.059	0.099	0.200	0.000	0.272	0.090	0.607	1.000
$\|K\| = 4$	0.000	0.000	0.013	0.026	0.000	0.000	0.057	0.000	0.000

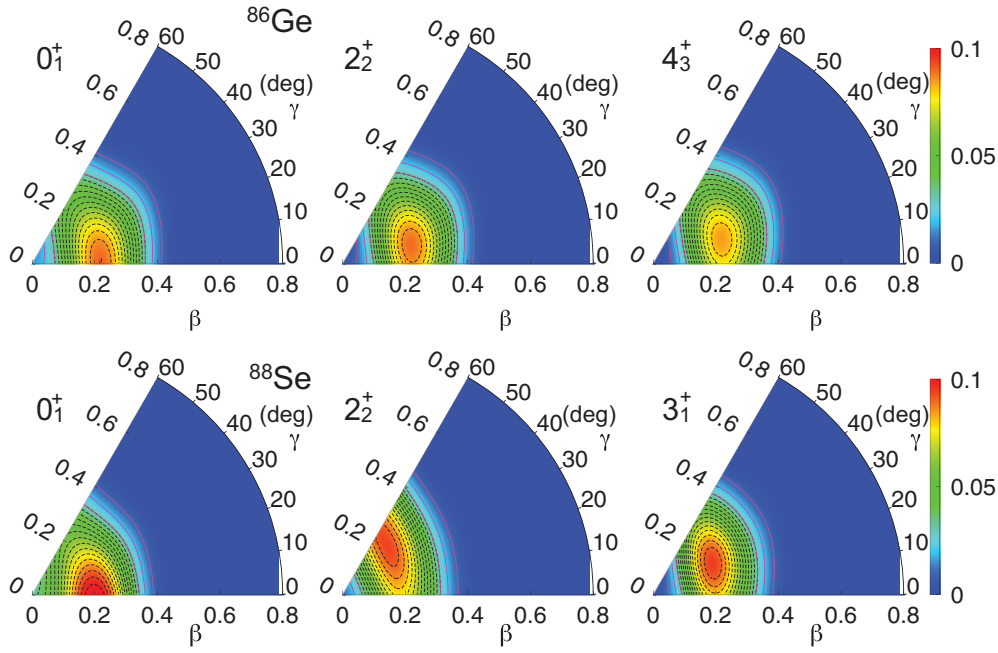

FIG. 4. (Color online) Collective wave functions for the band-head states of Fig. 3 in the (β, γ) plane. Upper and lower panels correspond to ^{86}Ge and ^{88}Se.

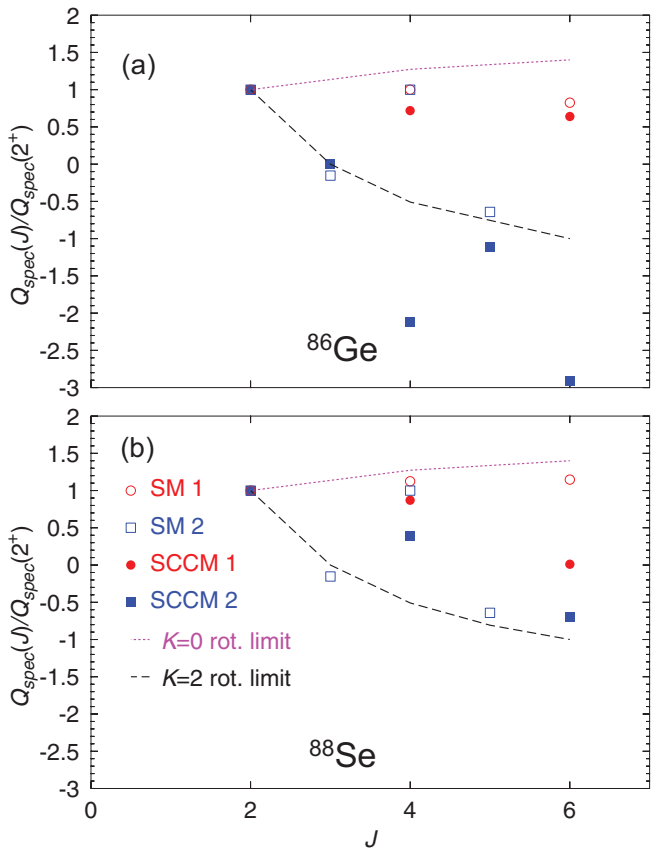

FIG. 5. (Color online) Spectroscopic quadrupole moments normalized to the value $Q_{\rm spec}(2_1^+)$ (g.s. band, bullets) and $Q_{\rm spec}(2_2^+)$ (first excited band, boxes) for (a) ^{86}Ge and (b) ^{88}Se. In lines, the rotor limit for $K = 0$ (dotted) and $K = 2$ (dashed) are given.

agreement is however expected since the effective charges in SM have been chosen so to reproduce the transition rates in the neighboring Zr isotones [1].

In spite of considerable differences in the absolute magnitude of $B(E2)$ values, it is conspicuous that both models predict the largest $B(E2)$ value between the first 3^+ and the second excited 2^+ states in ^{86}Ge. The level sequence and transition rates obtained in both models suggest that ^{86}Ge can be non-axially deformed. Other characteristic features common to triaxial nuclei appear in both calculations for ^{86}Ge: the $Q_{\rm spec}$ values of the first 2^+ and the second 2^+ have the same value but the opposite sign and $Q_{\rm spec}(3^+) \sim 0$ (see Tables III, V, VII).

In ^{88}Se, shell model predicts more deformed structure with a lower lying 2^+ state than SCCM, though the difference is of only 200 keV. A possible experimental candidate for 2^+ state is located at 886 keV according to Ref. [31], SMMC appears thus to be closer to the measurement. However, recently a different value (651 keV) of 2^+ energy in ^{88}Se has been reported [32], which agrees perfectly with the shell model prediction and points to a stronger deformation of this nucleus than obtained in the SCCM model. The remaining yrast levels and the excited bands are located much higher in energy in SMMC calculations than in SM. Both models predict a much more complicated band structure in this nucleus. As previously, transition rates between the yrast and excited bands are relatively small in shell model, while SCCM calculations predict considerable transitions between them.

The major difference in the two models concerns the degree of deformation of both nuclei. While the SCCM calculation find ^{88}Se more spherical than ^{86}Ge, the shell model predicts a larger spectroscopic moment in Se than in Ge, which follows

the pseudo-SU(3) scheme. It can be clearly seen in Fig. 5 that shell model results follow more closely the rotational limit for the ground state and excited bands in both ^{86}Ge and ^{88}Se than the SCCM ones. Interestingly, SCCM supports shell model findings that the triaxiality is more important in ^{86}Ge and ^{88}Se and both models predict much a lower $B(E2; 3^+ \rightarrow 2_2^+)$ value in ^{88}Se. In addition, both models also agree that the $K = 2$ bands do not continue to the second excited 4^+ state in ^{86}Ge and ^{88}Se nuclei.

IV. CONCLUSIONS

We have analyzed the quadrupole properties of neutron rich nuclei, just above the $N = 50$ shell closure. We have employed the algebraic pseudo-SU(3) model, shell model framework with empirically adjusted interactions in a $\pi r3g - \nu r4h$ model space outside the ^{78}Ni core and finally, the particle and angular momentum symmetry conserving beyond-mean field calculations with Gogny forces. The pseudo-SU(3) and shell model results appear to be in a good qualitative and quantitative agreement. Both models predict the signs of deformation in Se and Ge nuclei with four neutrons above the $N = 50$ shell closure. The beyond mean-field calculations agree well with the shell model ones in their predictions of energy levels and band structures of ^{86}Ge. The models used in this work consistently indicate that a maximum of triaxiality can appear in ^{86}Ge, where a low lying 3^+ level connected by a strong transition to the 2_2^+ should be observed. However, some discrepancies are found in the two approaches for ^{88}Se, where shell model calculation envisage stronger deformation effects than SCCM calculations. Further theoretical efforts are required to understand their origin. It is now a challenge for future experiments to verify the degree of collectivity around the $N = 50$ shell closure and wether the triaxiality can indeed develop in the nuclei just above the magic ^{78}Ni.

ACKNOWLEDGMENTS

T.R.R. acknowledges support from BMBF-Verbundforschungsprojekt no. 06DA7047I and Helmholtz International Center for FAIR program. K.S. and T.R.R. acknowledge the support from the French-German IN2P3-GSI 10-63 collaboration agreement.

[1] K. Sieja, F. Nowacki, K. Langanke, and G. Martinez-Pinedo, Phys. Rev. C **79**, 064310 (2009).
[2] K. Sieja and F. Nowacki, Phys. Rev. C **81**, 061303(R) (2010).
[3] K. Sieja and F. Nowacki, Phys. Rev. C **85**, 051301(R) (2012).
[4] http://www-phynu.cea.fr/.
[5] M. Bender and P.-H. Heenen, Phys. Rev. C **78**, 024309 (2008).
[6] J. M. Yao, H. Mei, H. Chen, J. Meng, P. Ring, and D. Vretenar, Phys. Rev. C **83**, 014308 (2011).
[7] T. R. Rodríguez and J. L. Egido, Phys. Rev. C **81**, 064323 (2010).
[8] J. Van de Walle *et al.*, Phys. Rev. C **79**, 014309 (2009).
[9] M. Lebois, D. Verney, F. Ibrahim, S. Essabaa, F. Azaiez, M. C. Mhamed, E. Cottereau, P. V. Cuong, M. Ferraton, K. Flanagan *et al.*, Phys. Rev. C **80**, 044308 (2009).
[10] J. A. Winger *et al.*, Phys. Rev. C **81**, 044303 (2010).
[11] E. F. Jones, P. M. Gore, J. H. Hamilton, A. V. Ramayya, J. K. Hwang, A. P. deLima, S. J. Zhu, C. J. Beyer, Y. X. Luo, W. C. Ma *et al.*, Phys. Rev. C **73**, 017301 (2006).
[12] J. P. Delaroche, M. Girod, J. Libert, H. Goutte, S. Hilaire, S. Péru, N. Pillet, and G. F. Bertsch, Phys. Rev. C **81**, 014303 (2010).
[13] D. Verney, B. Tastet, K. Kolos, F. Le Blanc, F. Ibrahim, M. Cheikh Mhamed, E. Cottereau, P. V. Cuong, F. Didierjean, G. Duchêne *et al.*, Phys. Rev. C **87**, 054307 (2013).
[14] T. Rząca-Urban *et al.*, Phys. Rev. C **88**, 034302 (2013).
[15] E. Caurier, G. Martinez-Pinedo, F. Nowacki, A. Poves, and A. P. Zuker, Rev. Mod. Phys. **77**, 427 (2005).
[16] A. F. Lisetskiy, B. A. Brown, M. Horoi, and H. Grawe, Phys. Rev. C **70**, 044314 (2004).
[17] A. Gniady, E. Caurier, F. Nowacki, and A. Poves (unpublished).
[18] E. Caurier, F. Nowacki, A. Poves, and K. Sieja, Phys. Rev. C **82**, 064304 (2010).
[19] K. Sieja, G. Martinez-Pinedo, L. Coquard, and N. Pietralla, Phys. Rev. C **80**, 054311 (2009).
[20] W. Urban *et al.*, Phys. Rev. C **79**, 044304 (2009).
[21] T. Rzaca-Urban, K. Sieja, W. Urban, F. Nowacki, J. L. Durell, A. G. Smith, and I. Ahmad, Phys. Rev. C **79**, 024319 (2009).
[22] W. Urban, K. Sieja, G. S. Simpson, T. Soldner, T. Rzaca-Urban, A. Złomaniec, I. Tsekhanovich, J. A. Dare, A. G. Smith, J. L. Durell *et al.*, Phys. Rev. C **85**, 014329 (2012).
[23] G. S. Simpson, W. Urban, K. Sieja, J. A. Dare, J. Jolie, A. Linneman, R. Orlandi, A. Scherillo, A. G. Smith, T. Soldner *et al.*, Phys. Rev. C **82**, 024302 (2010).
[24] M. Czerwinski *et al.*, Phys. Rev. C (to be published).
[25] E. Caurier and F. Nowacki, Acta Phys. Pol. B **30**, 705 (1999).
[26] K. Kumar, Phys. Rev. Lett. **28**, 249 (1972).
[27] A. Arima, M. Harvey, and K. Shimizu, Phys. Lett. B **30**, 517 (1969).
[28] P. Ring and P. Schuck, *The Nuclear Many-Body Problem* (Springer-Verlag, Berlin, 1980).
[29] M. Anguiano, J. Egido, and L. Robledo, Phys. Lett. B **545**, 62 (2002).
[30] A. Davydov and G. Filippov, Nucl. Phys. **8**, 237 (1958).
[31] http://www.nndc.bnl.gov/.
[32] J. Pereira, presented at the April Meeting of the American Physical Society, Denver, Colorado, US, April 2013.